Electronic Supplementary Information

A Zn-nitrite battery as an energy-output electrocatalytic system for high-efficiency ammonia synthesis by carbon-doped cobalt oxide nanotubes

Rong Zhang,[1] Shaoce Zhang,[1] Ying Guo,[1] Chuan Li,[1] Jiahua Liu,[1] Zhaodong Huang,[1] Yuwei Zhao,[1] Yangyang Li,[1] Chunyi Zhi[1,2*]

[1]Department of Materials Science and Engineering, City University of Hong Kong, 83 Tat Chee Avenue, Kowloon, Hong Kong 999077, Hong Kong

[2]Centre for Functional Photonics, City University of Hong Kong, Kowloon, Hong Kong

Corresponding author: Prof. Chunyi Zhi

Email: cy.zhi@cityu.edu.hk

S1. Experiment section

Chemicals

Potassium sulfate (K_2SO_4, 99%), potassium nitrite (KNO_2, 99.99%), hydrazine monohydrate ($N_2H_4 \cdot H_2O$, > 98%), Deuterium oxide (D_2O, 99.9 atom % D), hydrochloric acid (HCl, 37%), sodium hydroxide (NaOH, > 98%), cobalt chloride hexahydrate ($CoCl_2 \cdot 6H_2O$, > 99%), sodium oxalate ($Na_2C_2O_4$, 99%), hydrogen peroxide (H_2O_2, 30%), sodium hypochlorite solution (NaClO, available chlorine 4.0 %), p-Dimethylaminobenzaldehyde ($C_9H_{11}NO$), salicylic acid ($C_7H_6O_3$, 99%), ethanol (C_2H_5OH, 99.7%), polyvinyl pyrrolidone (PVP), trisodium citrate ($C_6H_5Na_3O_7$, 98%), sodium nitroferricyanide dehydrate ($C_5FeN_6Na_2O \cdot 2H_2O$, 99%), ethylene glycol ($C_2H_8O_2$, 99%) were purchased from Shanghai Macklin Biochemical Co., Ltd. W1S1005 carbon cloth (CC) was purchased from Fuel Cell Store Ltd. Bipolar membrane (Fumasep® FBM) was purchased from Fumatech GmbH. A commercial Nafion 117 membrane and typical Nafion solution (5 wt.%) was purchased from DuPont™ (E. I. du Pont de Nemours and Company).

Synthesis of the $C_2O_4^{2-}$ doped CoC_2O_4 precursor

Typically, 2 mmol of $CoCl_2 \cdot 6H_2O$ and 8 mmol of $Na_2C_2O_4$ were dissolved in 40 mL of ethylene glycol to form a homogeneous solution under continuous magnetic stirring. The solution was then transferred to a 50 mL Teflon-lined autoclave. The reactor was sealed and kept at 200 °C for 16 h in the oven. After the reaction was completed, the

pink-colored precipitate was collected by centrifugation, washed with deionized water and ethanol for several times, and dried in a vacuum oven at 60 °C for 12 h.

Synthesis of the Co_3O_4 and C/Co_3O_4

Briefly, 2 g of PVP (M_W = 1 300 000) was added into 30 mL of ethanol. After 1 h stirring, 0.4 g of the obtained $C_2O_4^{2-}$ doped CoC_2O_4 was dispersed into the above solution. After 12 h stirring, the $C_2O_4^{2-}$ doped CoC_2O_4/PVP complex was harvested by centrifugation and dried at 60 °C for 12 h. To obtain C/Co_3O_4, the $C_2O_4^{2-}$ doped CoC_2O_4/PVP complex was transferred into a box furnace and annealed in air at 400 °C for 2 h with a heating rate of 2 °C min^{-1}. Undoped Co_3O_4 was prepared by calcinating $C_2O_4^{2-}$ doped CoC_2O_4 nanorods directly in air at 400 °C for 2 h.

Characterization

The crystalline, morphologies and microstructures of samples were investigated by XRD using a Bruker D2 Phaser diffractometer with Cu Kα irradiation (λ = 1.54 Å), field-emission scanning electron microscopy (FEI Quanta 450 FEG) and JEOL-2001F field-emission TEM (JEOL-2001F). The surficial chemical states and compositions of the as-obtained products were investigated by XPS (ESCALB 250) with an Al Kα X-ray beam (E = 1486.6 eV). ^{1}H-NMR measurements were performed on Bruker 400MHz ASCEND AVANCE III HD Nuclear Magnetic Resonance System (NMR-400). UV-Vis spectroscopy measurements were carried out using a UV/Vis Spectrometer DB-20. FTIR measurements were carried out using Spectrum Two FTIR Spectrometers by PerkinElmer. KPFM experimental results were obtained by Bruker Dimension Icon.

Computational Details

All the computations were conducted based on the density functional theory (DFT) using the Cambridge Sequential Total Energy Package (CASTEP) code of the Materials Studio 2018 software. The generalized gradient approximation (GGA) with the Perdew-Burke-Ernzerhof (PBE) functional were used to describe the electronic exchange and correlation effects. The kinetic-energy cutoff was set as 500 eV. The geometry optimization within the conjugate gradient method was performed with forces on each atom less than 0.05 eV/Å. An energy tolerance is 5.0×10^{-6} eV per atom, and a maximum displacement of 0.001Å was considered. A Co_3O_4 (311) surface with a three-layer model of the crystal plane composed of 54 atoms was used for calculation with a sufficient vacuum gap of 15 Å. Bottom atomic Co-O layer was fixed while other layers and the adsorbates were fully relaxed during structural optimizations. The free energies for each reaction were given after correction: $\Delta G = \Delta E - T\Delta S$. Where ΔE is the reaction energy obtained by the difference between reactants and products; ΔS is the change in entropy for each reaction. Entropy values are taken from the standard database in the NIST webbook (J. Phys. Chem. Ref. Data 1996, 25, 551- 603.). The entropies of adsorbate and adsorption site are negligible.

Electrochemical measurements

Before the NO_2^-RR tests, the Nafion 117 membrane was pretreated in 5 wt% H_2O_2 aqueous solution at 80 °C for 1 h and then in ultrapure water at 80 °C for another 1 h. All electrochemical measurements were carried out in the argon atmosphere. The CC-supported catalysts (1 × 1 cm^2), Ag/AgCl (3 M KCl), and graphite rod were used as the

work electrode, the reference electrode and the counter electrode, respectively. For the preparation of the working electrode, 10 mg of samples was dispersed in 0.95 mL of isopropyl alcohol and 50 μL of 0.25% Nafion solution. The mixed solution was sonicated for 30 min to form a homogeneous ink. 50 μL of the catalyst ink was drop cast onto CC (1×1 cm^2) and dried at room temperature with a loading mass of 0.5 mg/cm^2. All electrochemical tests were carried out at ambient conditions. LSV tests were conducted with the scan rate of 5 mV/s in the three-electrode system. The chronoamperometry tests were conducted at a series of applied potentials in a typical H-type cell that contains 50-mL electrolyte separated by a membrane (Nafion 117) on the electrochemical workstation (CHI 760E, Chenhua, China). All potentials in this work refer to RHE, E(RHE) = E(Ag/AgCl) + 0.222 + 0.059pH. Different sweep rates in cyclic voltammetry measurements were performed and a linear relation was demonstrated on the basis of the current densities (J_{anodic}-$J_{cathodic}$) at the midpoint of the sweep voltage interval against scan rate. The C_{dl} was then obtained by halving the slope and the ECSA could be calculated by the following formula: ECSA = (C_{dl}/Cs) × S in which Cs and S respectively represent the specific capacitance (0.04 mF cm^{-2}) and the area of electrode (1 cm^2).

Assembly of the Zn-NO_2^- battery and electrochemical test.

The CC-supported catalysts (1 cm^2) and Zn plate (1 cm^2) were employed as the cathode for zinc-nitrate battery. A typical H-type cell that contains 20-mL cathode electrolyte (0.5 M K_2SO_4 + 50 mM KNO_2) and 20-mL anode electrolyte (1 M KOH). Considering our Zn-NO_2^- battery has an alkali anodic electrolyte and a neutral cathodic electrolyte,

a bipolar membrane consisting of an anion exchange layer and a cation exchange layer is used in the Zn-nitrite battery, where H^+ and OH^- are carriers at the cathode and anode, respectively. H^+ and OH^- ions migrate along the electric field to the corresponding electrodes and are consumed. The discharging polarization curves with a scan rate of 5 mV/s and galvanostatic tests were conducted using a CHI 760E workstation and Land 2001A battery test system at room temperature, respectively. After electrochemical test, the electrolyte was diluted for the next detection.

The power density (*P*) of zinc-nitrate battery was determined by $P = I \times V$, where *I* and *V* are the discharge current density and voltage, respectively.

The electrochemical reactions in Zn-nitrite battery are presented as following:

Cathode reaction: $NO_2^- + 6H_2O + 6e^- \rightarrow NH_4OH + 7OH^-$ (pH14) $E_0 = -0.160$ V

Cathode reaction: $NO_2^- + 6H_2O + 6e^- \rightarrow NH_4OH + 7OH^-$ (pH7) $E_0 = 0.340$ V

Cathode reaction: $NO_2^- + 8H^+ + 6e^- \rightarrow NH_4^+ + 2H_2O$ (pH0) $E_0 = 0.897$ V

Anode reaction: $3Zn + 6OH^- \rightarrow 3ZnO + 3H_2O + 6e^-$ $E_0 = -1.249$ V

Overall reaction: $3Zn + NO_2^- + 3H_2O \rightarrow 3ZnO + NH_4OH + OH^-$

$E_{Zn\text{-}nitrite\ battery} = 1.089$ V pH14

$E_{Zn\text{-}nitrite\ battery} = 1.589$ V pH7

$E_{Zn\text{-}nitrite\ battery} = 2.146$ V pH0

Though the Zn-NO_2^- battery system can simultaneously realize the NH_3 synthesis and electricity supply, the Zn dissolution and depletion of NO_2^- in the electrolyte will make the battery system less robust. To overcome the first problem, we can design a rechargeable Zn-NO_2^- battery to recycle Zn in the anodic chamber. However, the

oxygen evolution reaction ($4OH^- \rightarrow O_2 + 2H_2O + 4e^-$) and nitrite oxidation reaction ($NO_2^- + 2OH^- \rightarrow NO_3^- + H_2O + e^-$) may simultaneously occur in the cathode. The generated NO_3^- can then be reduced to NH_3 over the C/Co_3O_4 when discharging. Therefore, a selective electrocatalyst should be rationally designed. For the second problem, the flow system with continuously stirring can be introduced a steady NO_2^- concentration and a steady current density. Future research should be focused on designing and preparing efficient and selective electrocatalysts applied in a flow Zn-NO_2^- battery system.

Determination of ammonia

The amount of the produced NH_3 was detected with the indophenol blue method. To minimize the experimental error in quantification of ammonia, all data was recorded three times to obtain the error bar. In detail, a certain amount of electrolyte was taken out after NO_2^-RR test and diluted with electrolyte, and 1.25 mL of solution containing 0.625 M NaOH, 0.36 M salicylic acid and 0.17 M sodium citrate was added. Then 150 μL sodium nitroferricyanide solution (10 mg/mL) and 75 μL NaClO (available chlorine 4.0 wt%) solution were added. After 2 h under ambient conduction, UV-Vis absorption spectrum was recorded, and the absorbance value was obtained at the wavelength of 658 nm. The standard NH_4^+ solutions with the given concentrations of $(NH_4)_2SO_4$ in 0.5 M K_2SO_4 were prepared for building the calibration curve. The amount of the produced NH_3 was also determined by ^1H NMR. The pH value of the electrolyte after NO_2^-RR test was adjusted by 2 mol/L H_2SO_4 to achieve a weak acid. Then, 400 ppm of $C_4H_4O_4$ was added into the solution for a quantitative determination. Subsequently,

adding 50 μL D_2O into 0.5 mL of above mixture for NMR detection. Finally, the peak area ratio of NH_4^+ and $C_4H_4O_4$ was recorded and the concentration could be determined according to the standard calibration curves. The calibration curve was obtained by collecting the peak area ratios of NH_4^+ with given various concentrations and $C_4H_4O_4$ in 0.5 M K_2SO_4

Determination of hydrazine

Hydrazine in the electrolytes was also detected by the Watt-Chrisp method. A mixture of ethanol (100 mL), para(dimethylamino) benzaldehyde (2.0 g) and HCl (concentrated, 12 mL) were used as a color reagent. 2-mL color reagent was added into 2-mL of diluted electrolyte. After 30 min, the absorbance was measured at a wavelength of 458 nm. The standard hydrazine monohydrate solutions with the given concentrations of hydrazine in 0.5 M K_2SO_4 were also prepared for building the calibration curves.

Faradaic efficiency and ammonia yield rate

FEs and area-normalized yield rates of NH_3, NO_2^-, and N_2H_4 were calculated:

$$\text{FE } (NH_3) = (6F \times C \times V \times n) / Q$$

$$\text{Yield rate } (NH_3) = (C \times V \times n) / (t \times A)$$

$$\text{FE } (N_2H_4) = (12F \times C \times V \times n) / Q$$

$$\text{Yield rate } (N_2H_4) = (C \times V \times n) / (t \times A)$$

Where F is the Faraday constant (96485 C/mol), C is the measured NH_3 concentration, V is the volume of electrolyte, Q is the total charge passed through the electrode, n is the dilution factor and A is the geometer area of the working electrode (1×1 cm^2).

S2. Fig.s and tables

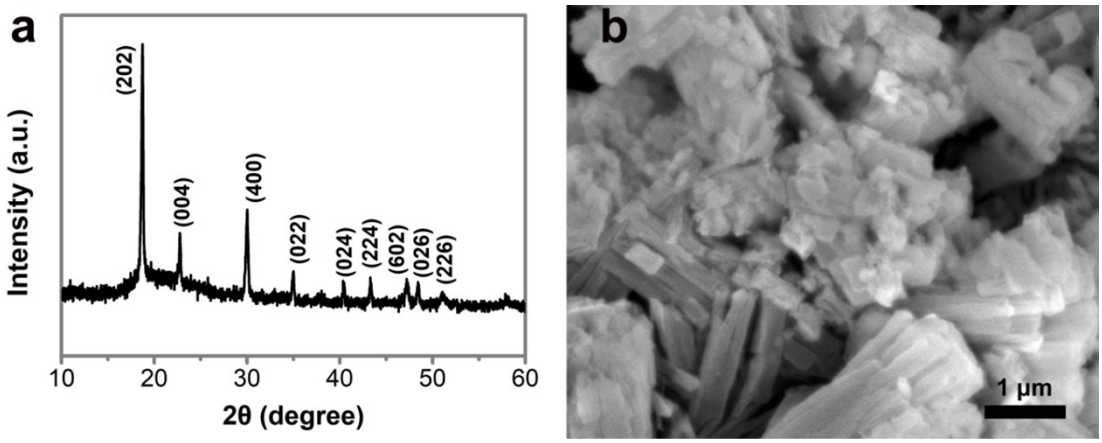

Fig. S1. XRD pattern and SEM image of $C_2O_4^{2-}$-doped CoC_2O_4.

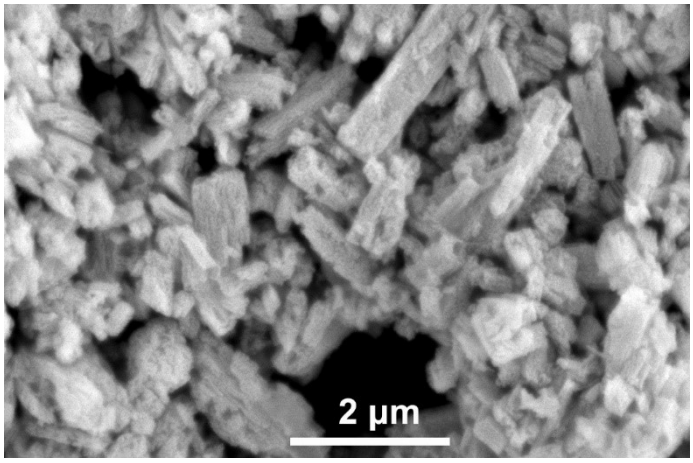

Fig. S2. SEM image of the C/Co_3O_4.

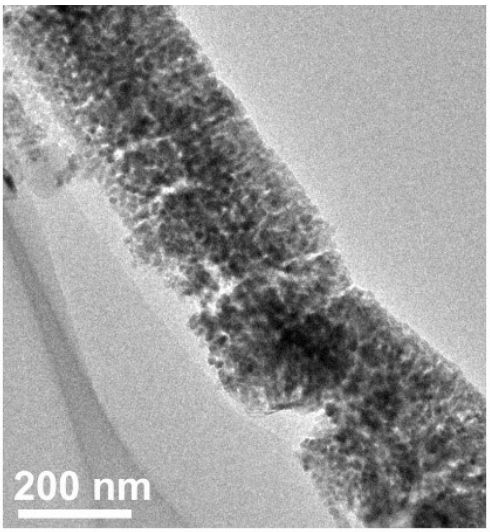

Fig. S3. TEM images of the Co_3O_4.

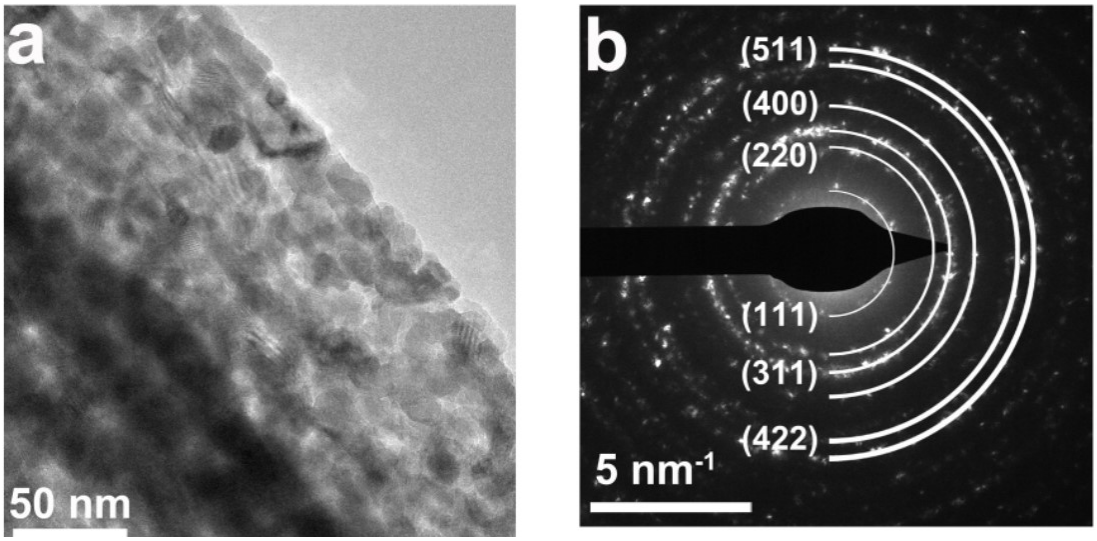

Fig. S4. (a) TEM images of the C/Co_3O_4 shell. (b) SEAD pattern of the C/Co_3O_4 nanocrystal.

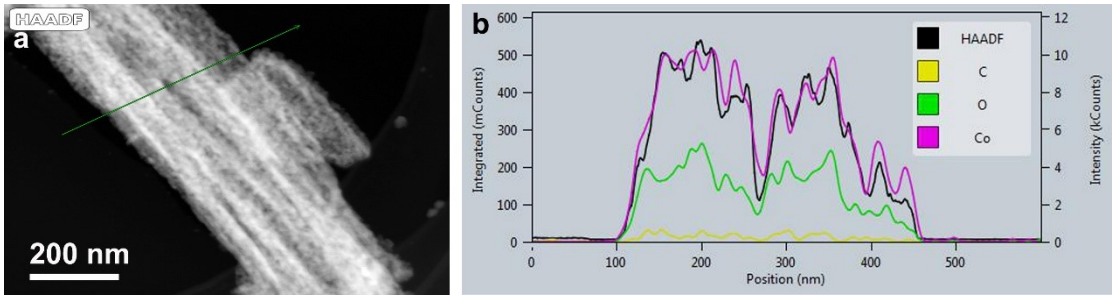

Fig. S5. EDS compositional line profile of C/Co_3O_4.

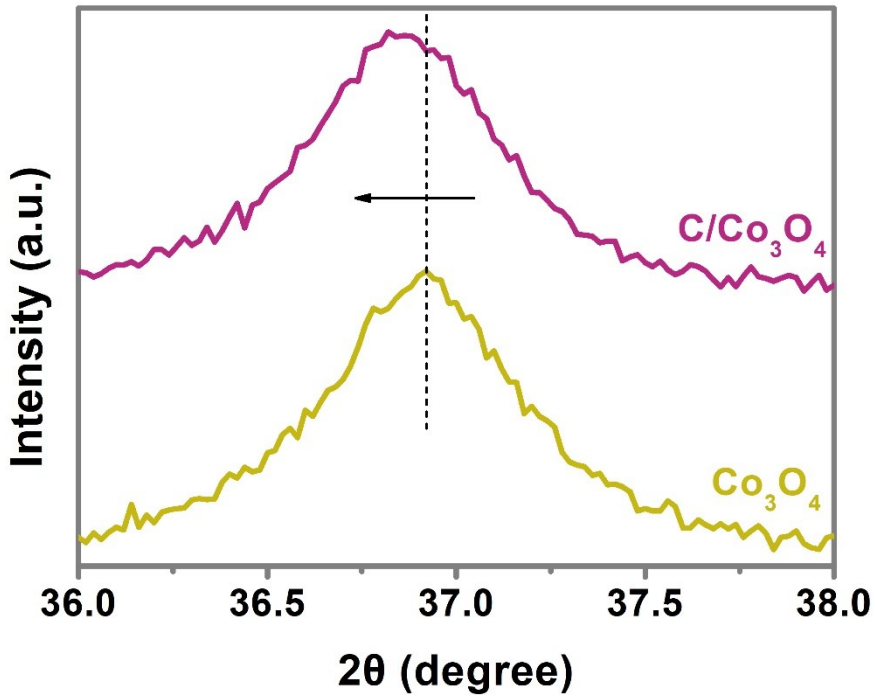

Fig. S6. Magnified view of the XRD patterns for doped and undoped Co_3O_4.

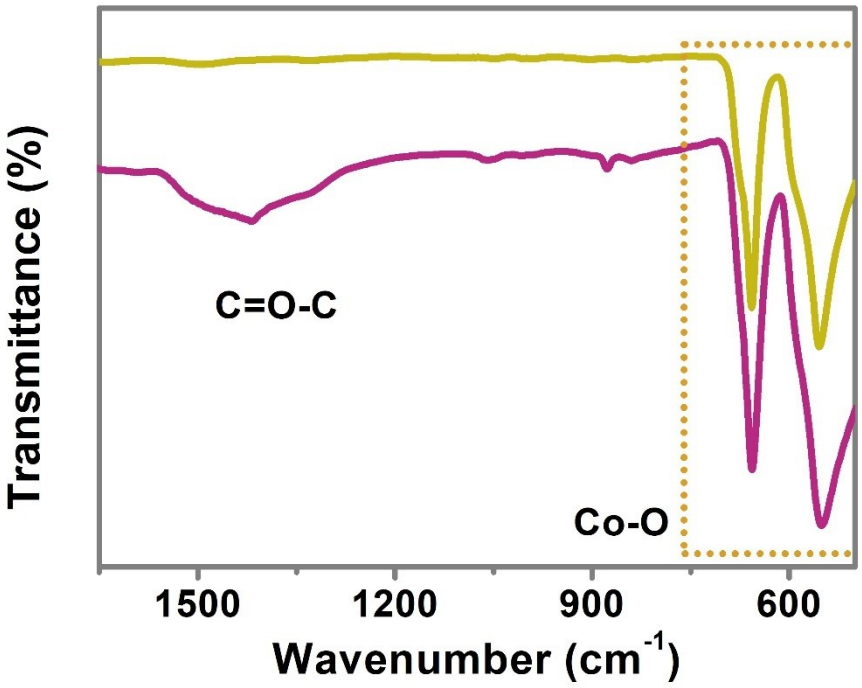

Fig. S7. FTIR spectra of the undoped Co_3O_4 and C-doped Co_3O_4.

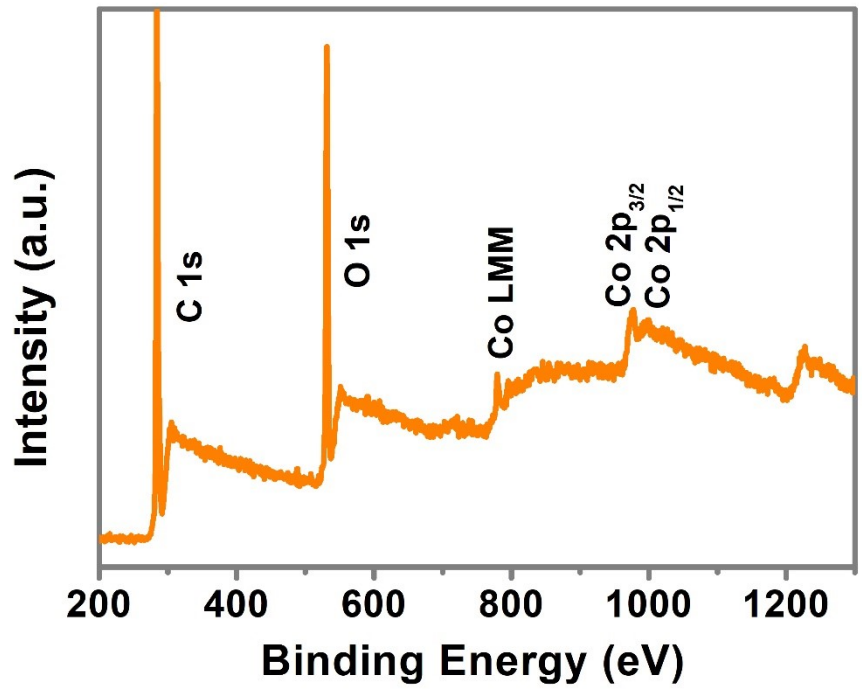

Fig. S8. XPS survey spectrum of the C/Co_3O_4.

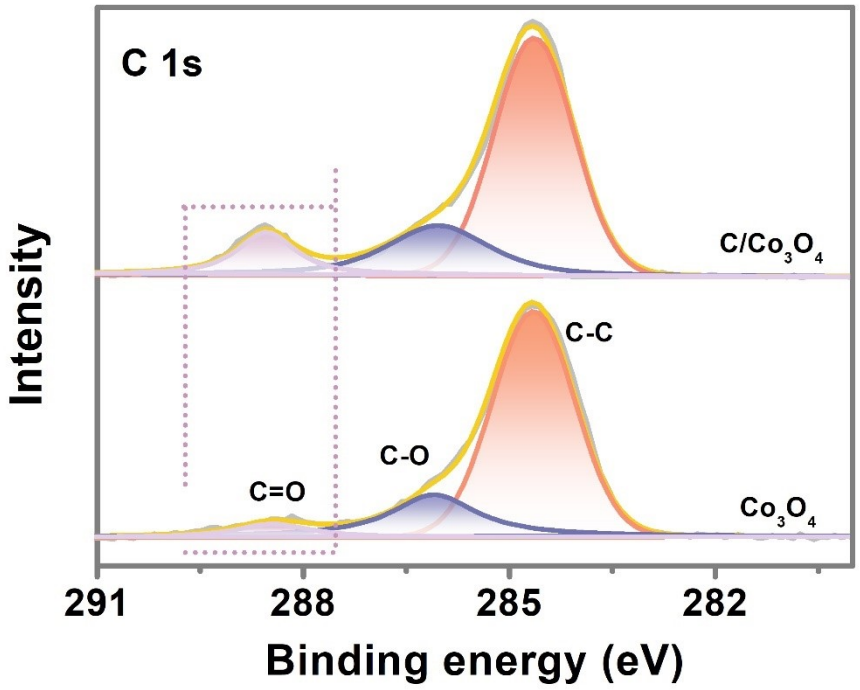

Fig. S9. XPS spectrum of the C/Co_3O_4 and Co_3O_4 in C 1s region.

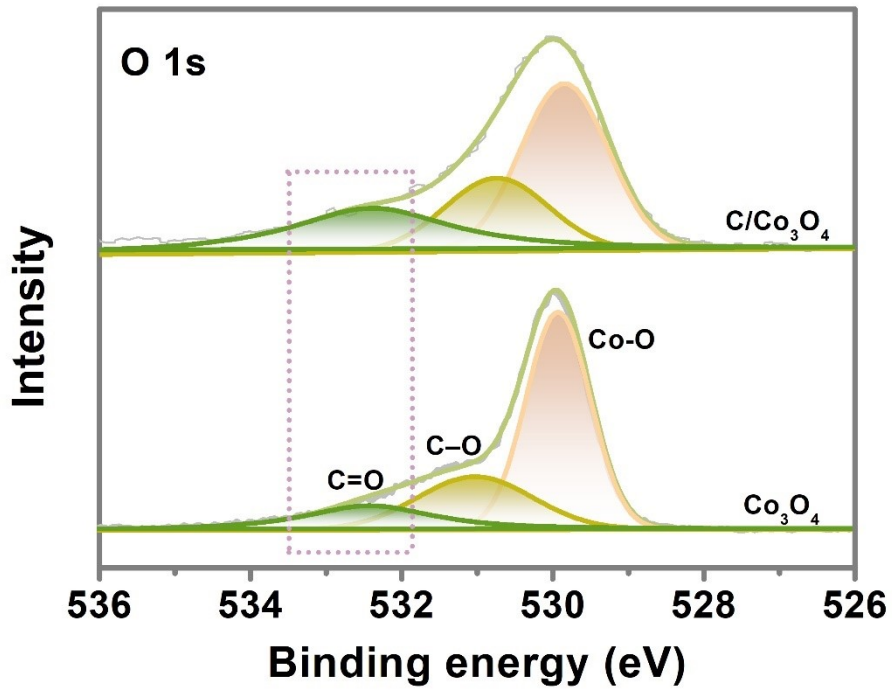

Fig. S10. XPS spectrum of the C/Co_3O_4 and Co_3O_4 in O 1s region.

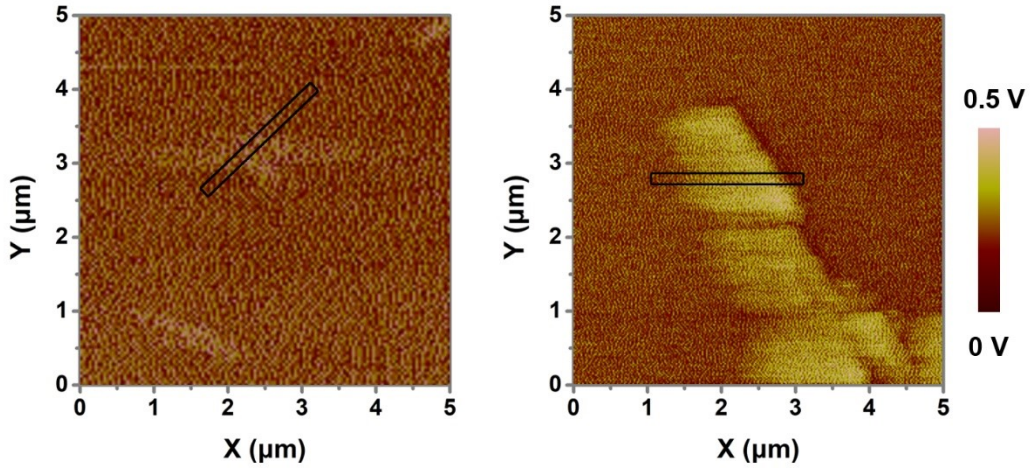

Fig. S11. KPFM images of the Co_3O_4 (left) and the C/Co_3O_4 (right).

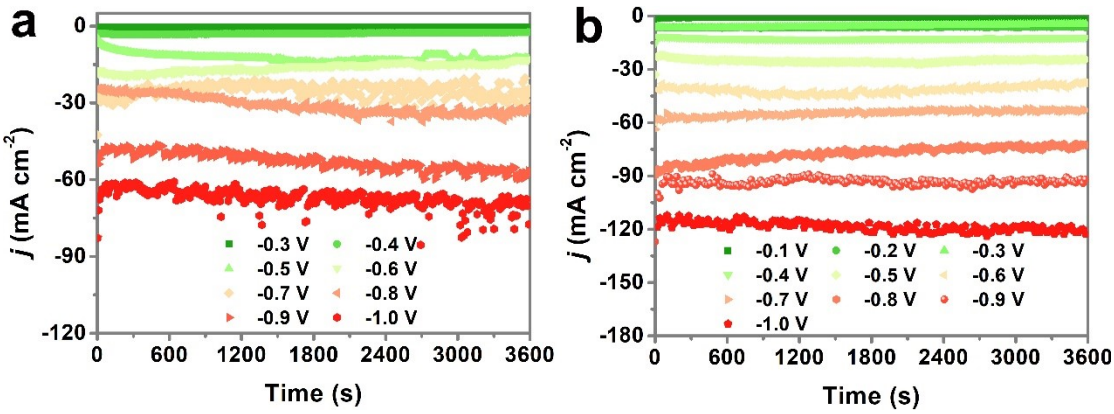

Fig. S12. Chronoamperometry curves of (a) Co_3O_4 and (b) C/Co_3O_4 in 0.5 M K_2SO_4 electrolyte with 50 mM KNO_2 at different potentials.

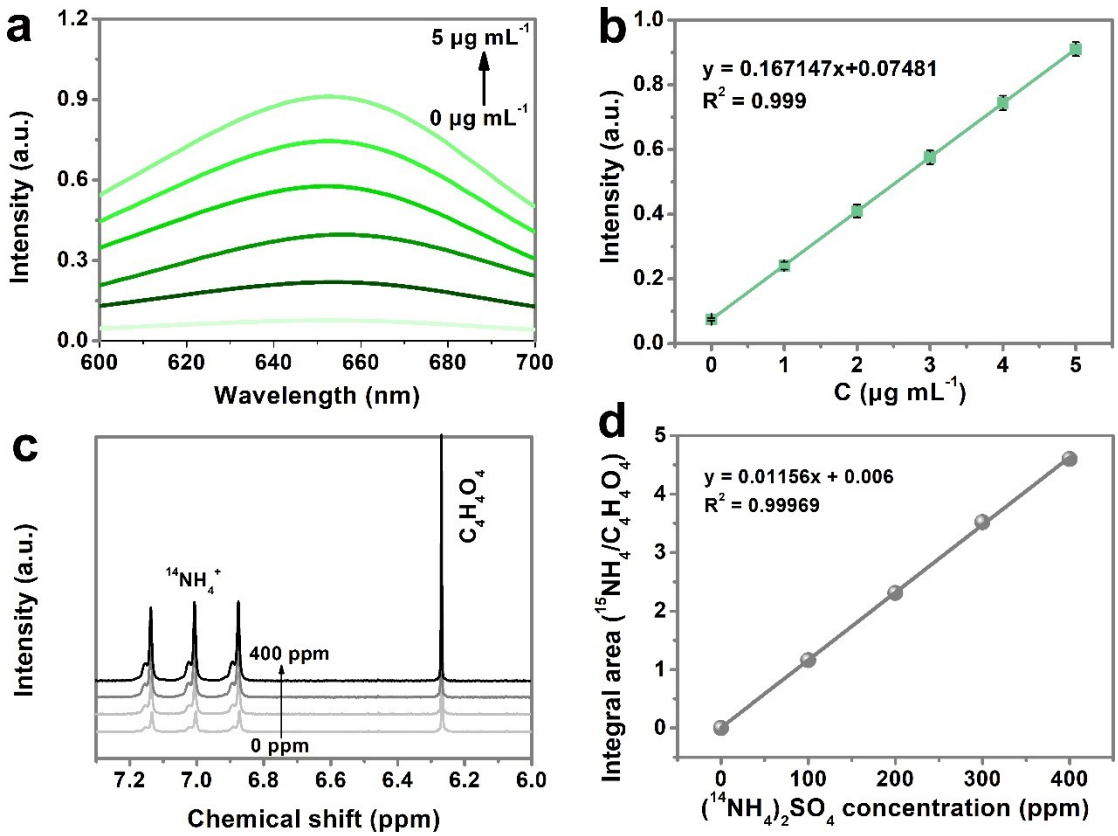

Fig. S13. (a) The UV-Vis adsorption curves and (b) calibration curve of the electrolyte with the given concentrations of $(NH_4)_2SO_4$. (c) ^1H NMR spectra of standard sample $(NH_4)_2SO_4$ solution with different concentrations. (d) Calibration curve of the electrolyte with the given concentrations of $(NH_4)_2SO_4$.

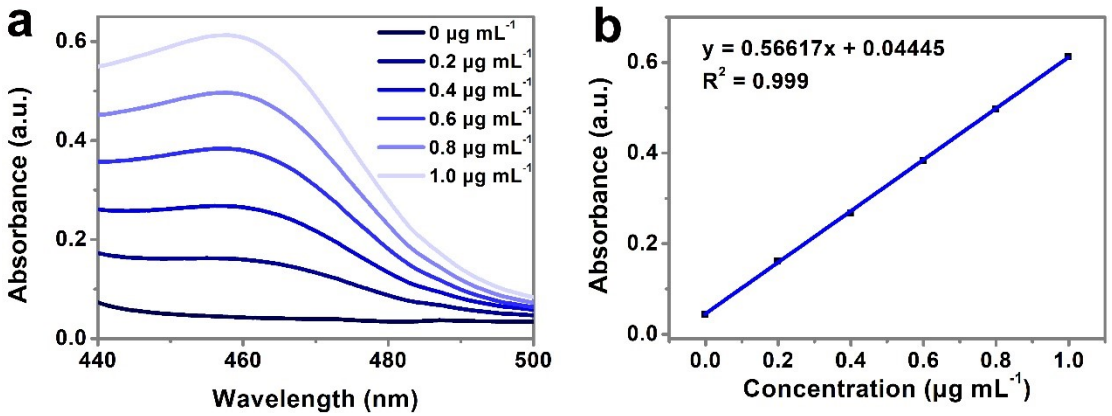

Fig. S14. (a)The UV-Vis adsorption curves and (b) Calibration curve of the electrolyte with the given concentrations of N_2H_4.

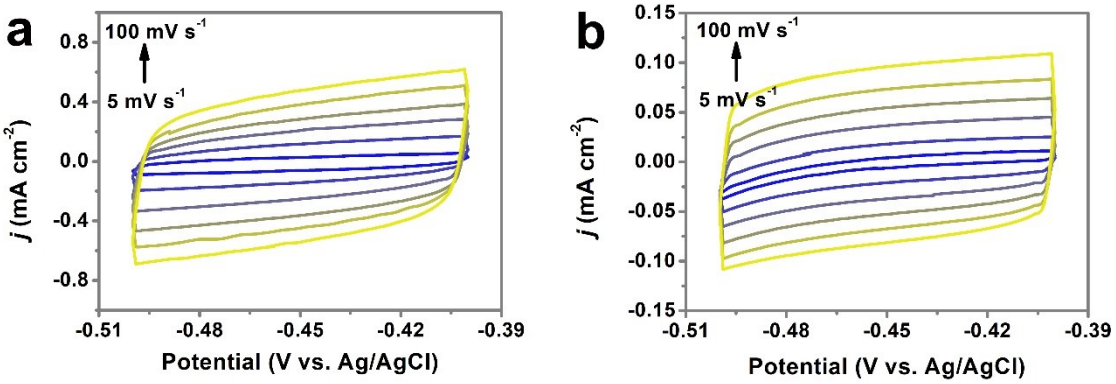

Fig. S15. The cyclic voltammetry profiles obtained on the (a) Co_3O_4 and (b) C/Co_3O_4 at the sweep rates of 5, 20, 40, 60, 80 and 100 mV s^{-1}.

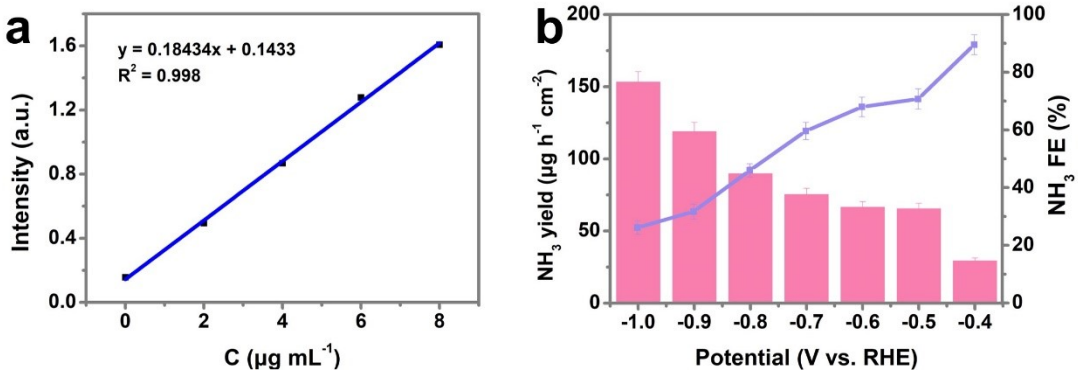

Fig. S16. Calibration curve in NH_3 measurement with different $(NH_4)_2SO_4$ concentration. (b) NH_3 yield and the corresponding FE of the C/Co_3O_4 catalyst for the NO_2^-RR in 0.5 M K_2SO_4 + 200 ppm NO_2^-.

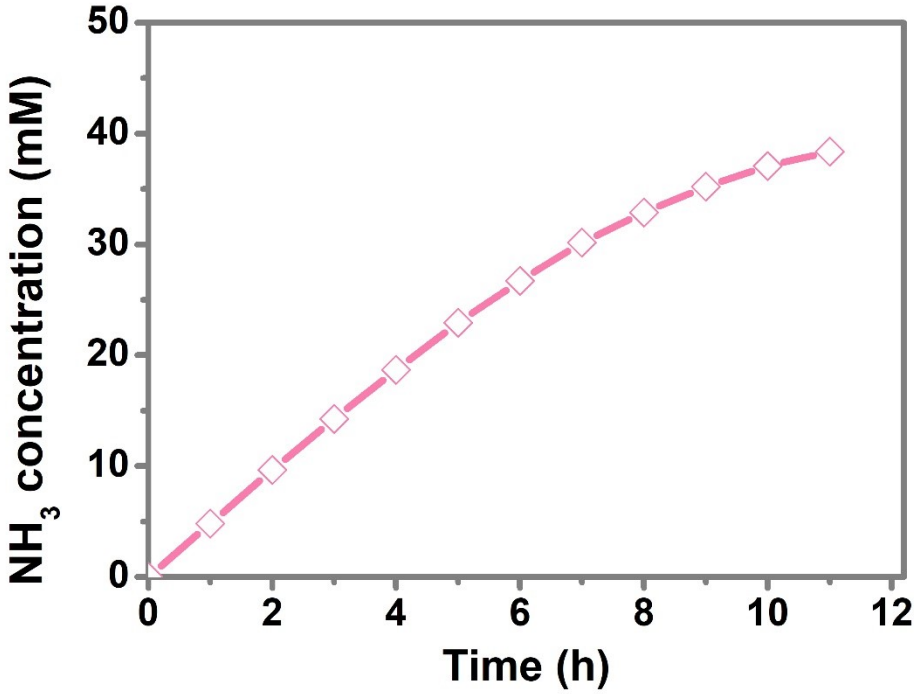

Fig. S17. The NH_3 concentration of the electrolyte after consecutive 12-h electrolysis.

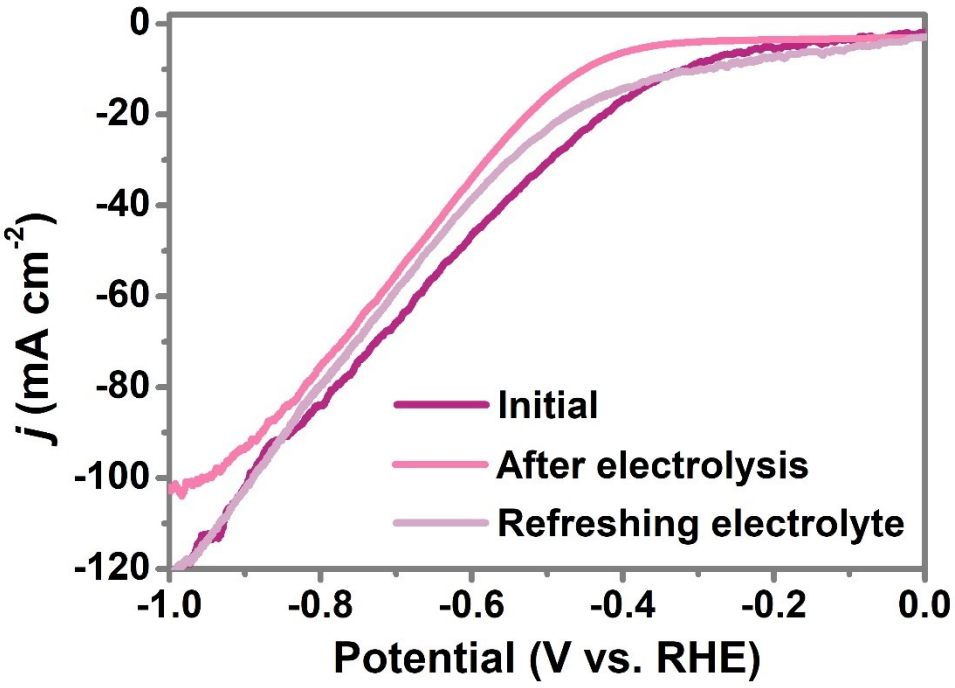

Fig. S18. LSV curves of the C/Co_3O_4 under different test conditions.

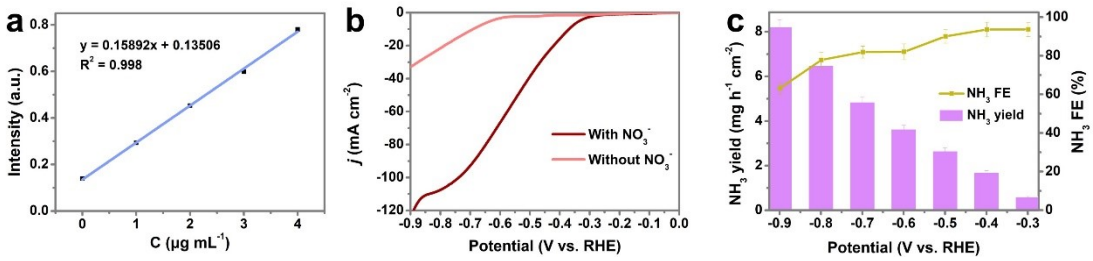

Fig. S19. (a) Calibration curve in NH_3 measurement with different $(NH_4)_2SO_4$. (b) Polarization curves of the C/Co_3O_4 in 0.5 M K_2SO_4 electrolyte with or without 50 mM NO_3^-. (c) NH_3 yield and NH_3 FE of the C/Co_3O_4 in 0.5 M K_2SO_4 with 50 mM NO_3^- electrolyte.

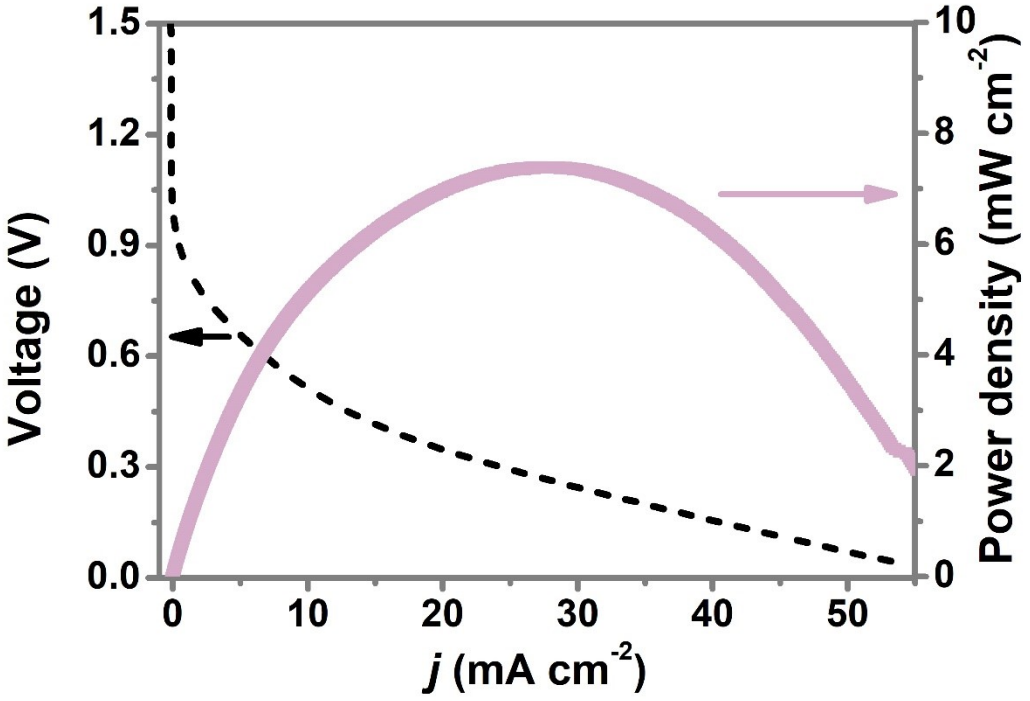

Fig. S20. Discharge polarization curves and the corresponding power density of the C/Co_3O_4-based Zn-NO_2^- battery with a Nafion 117 membrane.

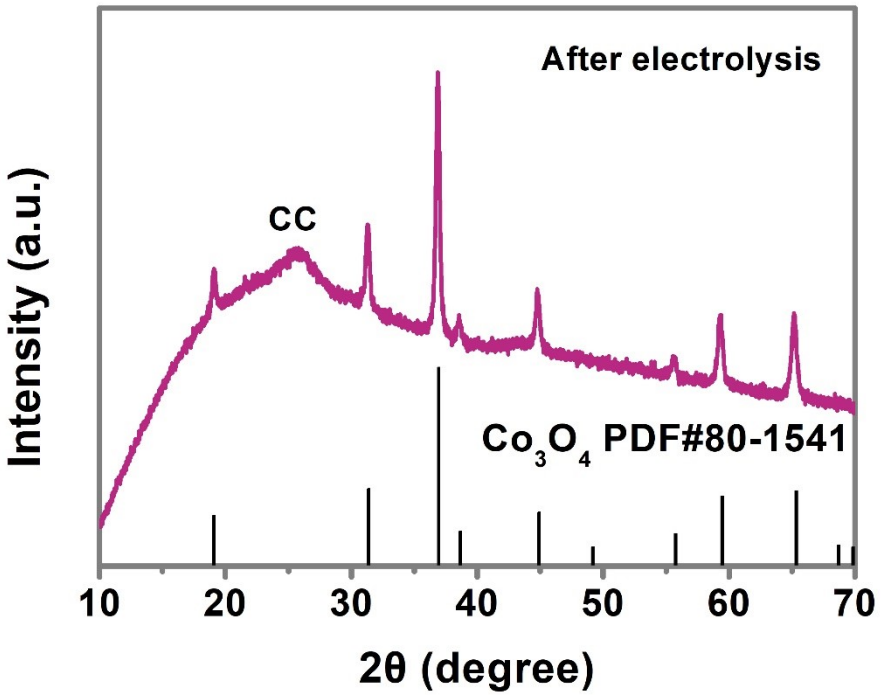

Fig. S21. XRD pattern of the C/Co_3O_4 after stability operation.

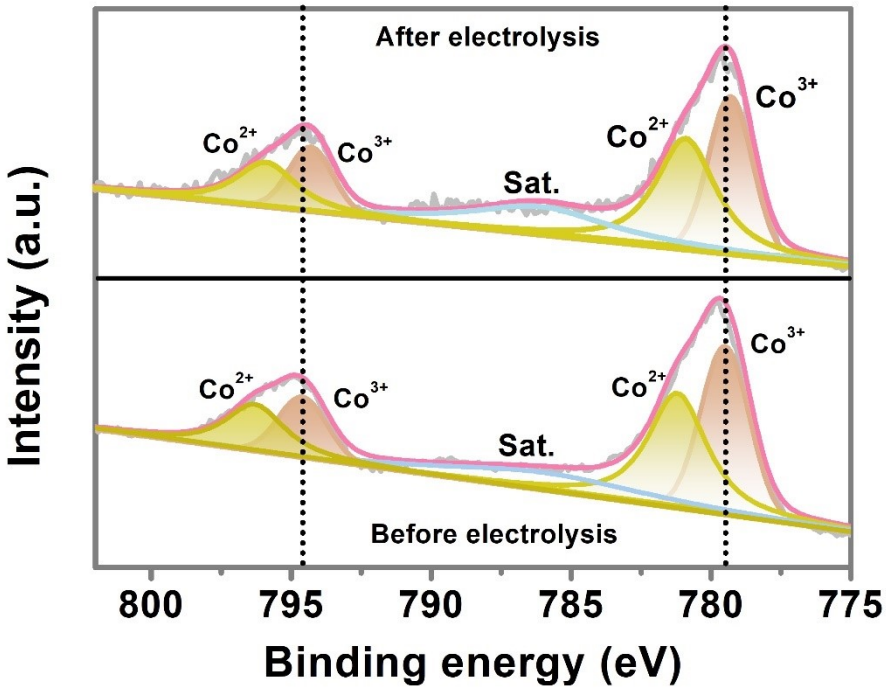

Fig. S22. XPS spectra of the C/Co_3O_4 in the Co 2p region before and after stability operation.

Table S1. The comparison of NH_3 synthesis performance of NRR electrocatalysts and C/Co_3O_4.

Reactions	Catalysts	NH_3 FE (%)	NH_3 Yield ($mg \cdot cm^{-2} \cdot h^{-1}$)	Ref.
NRR	B_4C	15.95	25.67	[1]
	$W_{18}O_{49}$-16Fe	20	24.7	[2]
	Cu–TiO_2	21.99	21.31	[3]
	SA Ru-Mo_2CT_x	25.77	40.57	[4]
	CoPc NTs	27.7	107.9	[5]
	Ru SAs/N-C	29.6	120.9	[6]
	Au nanocages	30.2	2.3	[7]
	CNT@C_3N_4–Fe&Cu	34	5.75	[8]
	Pd cubes	36.6	24.3	[9]
	RuFeCoNiCu/C	38.5	57.1	[10]
	PdH	43.6	0.0204	[11]
	Single Fe/N-C	56.55	7.48	[12]
	CN/C600	62.1	1.7	[13]
NO_2^-RR	**C/Co_3O_4**	**100**	**4.175**	**This work**

Table S2. The comparison of NH_3 synthesis performance of NO_3^-RR electrocatalysts and C/Co_3O_4.

Reaction	Catalysts	NH_3 FE (%)	NH_3 Yield ($mg \cdot cm^{-2} \cdot h^{-1}$)	Ref.
	Cu-Pd nanocube	97	0.997	[14]
NO_3^-RR	Cu/Cu_2O NWAs	81.2	0.1633	[15]
	Co_3O_4/Ti	80	0.634	[16]
	TiO_{2-x}	85	0.765	[17]
	Cu@$Cu_{2+1}O$ NWs	87.07	0.57653	[18]
	Pd/TiO_2	92.1	1.12	[19]
	Fe SAC	75	~1.955	[20]
	Ti	82	1.58	[21]
	OD-Ag	89	~1.25	[22]
	CoP PANSs	94	2.2	[23]
	Fe-PPy SACs	100	2.75	[24]
	Co/CoO NSAs	91.2	3.298	[25]
	Cu/Cu-Mn_3O_4	87.6	3.57	[26]
	Cu@Th-BPYDC	92.5	3.83	[27]
NO_2^-RR	**C/Co_3O_4**	**100**	**4.175**	**This work**

	Ni-NSA-V_{Ni}	89	0.236	[29]
	Cu_3P NA/CF	91.2	1.626	[30]
	CoP nanoarray	90	2.26	[31]
	Ni_2P/NF	90.2	2.6922	[32]
	Co@JDC	96.9	47.6	[33]
	FeOOH NTA/CC	94.7	11.937	[34]
NOR+NO_xRR	Co SAs/N-C	100	1.43	[35]
	Ni_3B@$NiB_{2.74}$	100	3.371	[36]
NORR	MoS_2 nanosheet	76.6	1.69	[37]
	$Ru_{0.05}Cu_{0.95}$	64.9	0.3	[38]
	Single atom Nb	77.1	5.018	[39]
	FeNC	5.1	0.343	[40]
	Cu foil	61.9	1.69	[41]
NO_2^-RR	**C/Co_3O_4**	**99.5**	**4.175**	**This work**

Table S3. The comparison of NH_3 synthesis performance of NO_2^-RR, NOR+NO_xRR and NORR electrocatalysts with C/Co_3O_4.

Table S4. The comparison of NH_3 synthesis performance of NORR electrocatalysts and C/Co_3O_4.

Batteries	**Cathode**	**OCV (V)**	**FE(%)**	**NH_3 Yield ($mg \cdot cm^{-2} \cdot h^{-1}$)**	**Power density ($mW\ cm^{-2}$)**	**Ref.**
$Na\text{-}N_2$	α-MnO_2 nanowire	-	26	-	-	[42]
$Al\text{-}N_2$	graphene/Pd	-	51.2	0.01084	-	[43]
$Li\text{-}N_2$	carbon cloth	-	59	-	-	[44]
$Li\text{-}N_2$	Mo_2C/NC	-	87	-	-	[45]
$Zn\text{-}N_2$	metallic copper	~0.5	59	-	0.0101	[46]
$Zn\text{-}N_2$	VN@NSC-900	~0.55	-	0.000172	0.01642	[47]
$Zn\text{-}N_2$	NbS_2	~1.3	-	0.0036	0.31	[48]
$Zn\text{-}N_2$	CoPi/NPCS	~1.4	16.35	0.0147	0.49	[49]
$Zn\text{-}N_2$	$Fe_{1.0}$HTNs	~0.6	-	0.000137	0.02765	[50]
$Zn\text{-}N_2$	Vs-FePS3 NSs	~1.75	-	-	2.6	[51]
$Zn\text{-}N_2$	CoPi/HSNPC	~1	24.42	-	0.31	[52]
$Zn\text{-}NO_3^-$	Pd/TiO_2	0.81	81.3	0.54	0.87	[53]
Zn-NO	MoS_2 nanosheets	2.03	85.0	0.4118	1.04	[54]
$Zn\text{-}NO_2^-$	**C/Co_3O_4**	**1.45**	**95.1**	**0.802**	**6.03**	**This work**

[1] Nat. Commun. 2018,9, 3485.

[2] Angew. Chem. Int. Ed. 2020, 59, 7356-7361.

[3] Adv. Mater. 2020, 32, 2000299.

[4] Adv. Energy Mater. 2020, 10, 2001364.

[5] ACS Nano 2021, 15, 3, 5230–5239.

[6] Adv. Mater. 2018, 30, 1803498.

[7] Nano Energy 2018,49, 316-323.

[8] Adv. Mater. 2020, 32, 2004382.

[9] Adv. Energy Mater. 2020, 10, 2002131

[10] Nat. Commun. 2019, 10, 3898.

[11] Angew. Chem. Int. Ed. 2019, 58, 18449-18455.

[12] Nat. Commun. 2019, 10, 341.

[13] Nano Lett. 2020, 20, 2879−2885.

[14] Nat. Energy 2020, 5, 605-613.

[15] Angew. Chem. Int. Ed. 2020, 59, 5350-5354

[16] Appl.Catal. B-Environ. 2019, 254, 391-402.

[17] ACS Catal. 2020, 10, 3533-3540.

[18] Chem. Eng. J. 2021, 426, 130759.

[19] Energy Environ. Sci. 2021, 14, 3938-3944.

[20] Nat. Commun. 2021, 12, 1-10.

[21] ACS Sustainable Chem. Eng. 2020, 8, 7, 2672–2681.

[22] ACS Catal. 2021, 11, 8431–8442.

[23] ACS Appl. Mater. Interfaces 2021, 13, 45521–45527.

[24] Energy Environ. Sci., 2021, 14, 3522-3531.

[25] Sci. China Chem. 2020, 63, 1469-1476.

[26] ACS Appl. Mater. Interfaces 2021, 13, 37, 44733–44741

[27] ACS Cent. Sci. 2021, 7, 6, 1066-1072.

[28] J. Am. Chem. Soc. 2018, 140, 16888–16892.

[29] J. Mater. Chem. A, 2021, 9, 239–243.

[30] Green Chem. 2021, 23, 5487-5493.

[31] DOI: 10.1007/s12274-021-3583-9.

[32] J. Colloid Interf. Sci. 2020, 606, 1055-1063.

[33] J. Mater. Chem. A, 2022, 10, 2842-2848.

[34] Chem. Commun., 2022, 58, 5160-5163.

[35] Appl. Catal. B: Environ. 2021, 299, 120667.

[36] Angew.Chem. Int. Ed. 2021, 60,14131–14137.

[37] Angew. Chem. Int. Ed. 2021, 60, 25263–25268.

[38] Sci. China. Chem. 2021, 64, 493–1497.

[39] Nano Energy 2020, 78, 105321.

[40] Nat. Commun. 2021, 12, 1856.

[41] Angew. Chem. Int. Ed. 2020, 59, 9711-9718.

[42] Energy Storage Mater. 2019, 23, 733–740.

[43] Energy Environ. Sci., 2020, 13, 2888-2895.

[44] Chem, 2017, 2, 525-532.

[45] Small Methods, 2019, 3, 1800334.

[46] Chem. Commun., 2019, 55, 12801-12804.

[47] Appl. Catal. B-Environ. 2021, 280, 119434.

[48] Appl. Catal. B-Environ., 2020, 270, 118892.

[49] ACS Appl. Mater. Interfaces 2021, 13, 12106–12117.

[50] J. Mater. Chem. A 2021, 9, 4026-4035.

[51] Nano Energy 2021, 81, 105613.

[52] J. Mater. Chem. A, 2021, 9, 11370-11380.

[53] Energy Environ. Sci., 2021, 14, 3938-3944.

[54] Angew. Chem. Int. Ed. 2021, 22, 25467-25472.